International Journal of Heat and Mass Transfer 52 (2009) 1945–1953

Contents lists available at ScienceDirect

International Journal of Heat and Mass Transfer

journal homepage: www.elsevier.com/locate/ijhmt

Magnetoconvection in a square cavity with partially active vertical walls: Time periodic boundary condition

N. Nithyadevi, P. Kandaswamy *, S. Malliga Sundari

UGC-DRS Centre for Fluid Dynamics, Department of Mathematics, Bharathiar University, Coimbatore 641 046, India

ARTICLE INFO

Article history:
Received 19 November 2007
Received in revised form 7 July 2008
Available online 13 December 2008

Keywords:
Magnetoconvection
Periodic boundary condition
Partially active walls
Square cavity
Control volume method

ABSTRACT

Magnetoconvection of an electrically conducting fluid in a square cavity with partially thermally active sidewalls is investigated numerically. Temperature of one of the thermally active regions of the side walls is periodic in time while the opposite wall is isothermal. The horizontal walls and the remaining parts of the side walls are thermally inactive. Nine different combinations of the relative positions of the active zones are considered. The governing equations are discretized by the control volume method with QUICK scheme and solved numerically by SIMPLE algorithm for the pressure–velocity coupling together with under relaxation technique. The tests were carried out for various values of amplitude, period, Grashof number, Hartmann number and Prandtl number. The heat transfer characteristics are presented in the form of streamlines, isotherms and velocity profiles both for transient and steady state. It is observed that the flow and the heat transfer rate in the cavity are affected by the sinusoidal temperature profile and by the magnetic field at lower values of Grashof number. The rate of heat transfer oscillates for increasing periods but it is maximum for $\Omega = 3$ and it is found to be an increasing function of amplitude but decreases for higher values of Hartmann number. The heat transfer rate is maximum for the middle–middle thermally active locations while it is poor for the top heating and bottom cooling active locations. The average Nusselt number decreases with an increase of Hartmann number and increases with increase of Prandtl number and Grashof number.

1. Introduction

Magnetoconvection in a cavity with time periodic thermal boundary conditions has many applications in industry, crystal growth techniques, space applications, etc. Unwanted convective flows can significantly be suppressed by applying an external magnetic field. Extensive studies have been made in recent years to examine the effects of magnetic field on the flow structure. Lage and Bejan [1] studied theoretically and numerically natural convection in a two-dimensional square cavity with one side cold and isothermal and the other side heated with pulsating heat flux. They observed that at sufficiently high Rayleigh number where convection is the heat transfer mechanism, the buoyancy-driven flow has the tendency to resonate to the periodic heating that is being supplied from the side.

Rudraiah et al. [2] investigated the effect of a magnetic field on free convection in a rectangular cavity. They found the effect of magnetic field is to decrease the rate of heat transfer. Kwak et al. [3] investigated the natural convection of an incompressible fluid in a square cavity having a hot sidewall with sinusoidally varying temperature. They found that the flow resonates with the internal gravity wave oscillations. Kandaswamy and Kumar [4] studied the natural convection of water near its density maximum in the presence of a uniform magnetic field. They observed that the effect of magnetic field on the natural convection is to inhibit the heat transfer rate. Oosthuizen and Paul [5] studied the natural convection flow in a square cavity with one of the vertical walls having two separate heating sections with spatially uniform but vary sinusoidally with time. They observed the flow to be essentially psuedo-steady for the dimensionless periods higher than 0.02 and periodic for dimensionless times greater than 0.4.

Kim et al. [6] studied the buoyant convection with internal heat generation under oscillating sidewall temperature of a cavity. They found that the secondary peak resonance is deducted for higher internal Rayleigh number. Saeid [7] numerically studied natural convection in a porous cavity with bottom wall heated with spatial sinusoidal temperature variation while the vertical walls are adiabatic. It is found that the average Nusselt number increases when the amplitude of the temperature variation increase. Crunkleton et al. [8] investigated the numerical simulation of periodic flow oscillation for low Prandtl number fluids in rectangular cavity. They found non-periodic flows for rectangular cavity with aspect ratio 2.0. Nithyadevi et al. [9] investigated the natural convection in a square cavity with partially thermally active side walls with periodic time variations. They found that the average heat transfer

* Corresponding author. Tel.: +91 422 2426764; fax: +91 422 2422387.
E-mail address: pgkswamy@yahoo.co.in (P. Kandaswamy).

0017-9310/$ - see front matter © 2008 Elsevier Ltd. All rights reserved.
doi:10.1016/j.ijheatmasstransfer.2008.08.039

Nomenclature

Alphabetics

a	amplitude
A	dimensionless amplitude
B_0	magnetic field
g	acceleration due to gravity
Gr	Grashof number
Ha	Hartmann number
L	length of the cavity
Nu	local Nusselt number
$\overline{Nu}$	average Nusselt number
p	pressure
Pr	Prandtl number
t	dimensional time
T	dimensionless temperature
u, v	velocity components
U, V	dimensionless velocity components
x, y	dimensional coordinates
X, Y	dimensionless coordinates

Greek symbols

α	thermal diffusivity
β	coefficient of thermal expansion
μ	dynamic viscosity
ν	kinematic viscosity
θ	temperature
ρ	density
σ_e	electrical conductivity of the medium
τ	dimensionless time
ω	dimensional period
Ω	dimensionless period

Subscripts

c	cold wall
h	hot wall
o	reference state

increases for increasing amplitude and for periods 1 and 5 and decreases for period 3.

Bilgen and Ben Yedder [10] studied the natural convection in a cavity with heating and cooling by sinusoidal temperature profiles on one sidewall and observed that the heat transfer is higher when the heated section is in the lower half of the cavity at high Rayleigh number. Cheikh et al. [11] investigated numerically the effect of aspect ratio on natural convection flow in a cavity submitted to periodic temperature boundary. For low values of period of the hot wall temperature, the amplitude became nearly constant at the cold wall. By increasing the period, the amplitude of the Nusselt number at the cold wall also increased until reaching the same value as the one at the hot wall.

Natural convection in a rectangular cavity with partially active vertical walls numerically studied by Nithyadevi et al. [12]. They showed that no remarkable change in the heat transfer rate is observed when the heating location is changed for a fixed cooling location. The heat transfer rate is enhanced when a cooling location is at the top of the cavity. Natarajan et al. [13] reported two-dimensional laminar natural convection flows in a trapezoidal cavity with uniform and non-uniform heating wall. The found that the non-uniform heating exhibits greater heat transfer rates at the center of the bottom wall than with uniform heating case for all Rayleigh number regimes.

Recently, a study of magnetoconvection in a cavity with partially active vertical walls was conducted by Kandaswamy et al. [14]. They showed that the heat transfer rate is maximum for the middle–middle thermally active locations while it is poor for the top–bottom thermally active locations. The average Nusselt number decreases with an increase of Hartmann number and increases with an increase of Grashof number. The present work deals with the effect of magnetic field on the flow and heat transfer in a square cavity with partially thermally active vertical walls with time periodic boundary conditions. In this study Hartmann number is varied from 0 to 100, Grashof number from 10^4 to 10^6 and Prandtl number from 0.054 to 2.05 with nine different relative positions of the thermally active locations.

2. Mathematical formulation

The unsteady two-dimensional natural convection flow in a square cavity of length L filled with an electrically conducting fluid is considered as shown in Fig. 1. A portion of the right wall is kept at a temperature θ_c and a portion of the left wall temperature is maintained periodic in time. The remaining boundaries of the cavity are thermally insulated. For nine different combinations of the thermally active locations (the hot region moving from top to bottom of the left wall and the cold region moving from bottom to top of the opposite wall) the heat transfer characteristics are investigated. The gravity acts vertically downwards. The uniform external magnetic field B_0 is applied parallel to gravity. It is assumed that the induced magnetic field is negligible compared to the applied magnetic field. Under the above assumptions, the conservation equations of mass, momentum and energy in a two-dimensional Cartesian coordinate system are

$$\frac{\partial u}{\partial x}+\frac{\partial v}{\partial y}=0 \tag{1}$$

$$\frac{\partial u}{\partial t}+u\frac{\partial u}{\partial x}+v\frac{\partial u}{\partial y}=-\frac{1}{\rho_0}\frac{\partial p}{\partial x}+\nu\nabla^2 u-\frac{\sigma_e B_0^2}{\rho_0}u \tag{2}$$

$$\frac{\partial v}{\partial t}+u\frac{\partial v}{\partial x}+v\frac{\partial v}{\partial y}=-\frac{1}{\rho_0}\frac{\partial p}{\partial y}+\nu\nabla^2 v-\frac{\rho}{\rho_0}g \tag{3}$$

$$\frac{\partial \theta}{\partial t}+u\frac{\partial \theta}{\partial x}+v\frac{\partial \theta}{\partial y}=\alpha\nabla^2\theta \tag{4}$$

where $\rho=\rho_0[1-\beta(\theta-\theta_c)]$

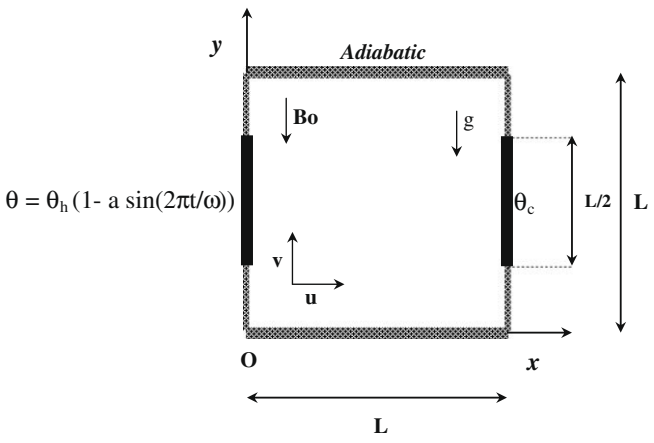

Fig. 1. Physical configuration.

The appropriate initial and boundary conditions are:

$t = 0$:	$u = v = 0$,	$\theta = \theta_c$,	$0 \leqslant x \leqslant L$,	$0 \leqslant y \leqslant L$,
$t > 0$:	$u = v = 0$,	$\frac{\partial\theta}{\partial y} = 0$,	$y = 0$ and L,	$0 \leqslant x \leqslant L$,
	$\theta = \theta_h(1 - asin(2\pi t/\omega))$		on the hot part,	$x = 0$,
	$\theta = \theta_c$,		on the cold part,	$x = L$,
		$\frac{\partial\theta}{\partial x} = 0$,	$x = 0$ and L,	$0 \leqslant y \leqslant L$.

where ω and a are the period and amplitude of oscillation of the hot wall temperature.

Introducing the following non-dimensional variables

$$\tau = \frac{t}{L^2/\nu}, \quad (X, Y) = \frac{(x, y)}{L}, \quad (U, V) = \frac{(u, v)}{\nu/L},$$
$$T = \frac{\theta - \theta_c}{\theta_h - \theta_c}, \quad \text{with } \theta_h > \theta_c$$

The non-dimensional form of Eqs. (1)–(4) are obtained as,

$$\frac{\partial U}{\partial X} + \frac{\partial V}{\partial Y} = 0 \tag{5}$$
$$\frac{\partial U}{\partial \tau} + U\frac{\partial U}{\partial X} + V\frac{\partial U}{\partial Y} = -\frac{\partial P}{\partial X} + \nabla^2 U - Ha^2 U \tag{6}$$
$$\frac{\partial V}{\partial \tau} + U\frac{\partial V}{\partial X} + V\frac{\partial V}{\partial Y} = -\frac{\partial P}{\partial Y} + \nabla^2 V + GrT \tag{7}$$
$$\frac{\partial T}{\partial \tau} + U\frac{\partial T}{\partial X} + V\frac{\partial T}{\partial Y} = \frac{1}{Pr}\nabla^2 T \tag{8}$$

The initial and boundary conditions in the dimensionless form are:

$\tau = 0$:	$U = V = 0$,	$T = 0$,	$0 \leqslant X \leqslant 1$,	$0 \leqslant Y \leqslant 1$,
$\tau > 0$:	$U = V = 0$,	$\frac{\partial T}{\partial Y} = 0$,	$Y = 0$ and 1,	$0 \leqslant X \leqslant 1$,
$T = 1 - A\,sin(\pi\tau/\Omega)$,		hot part	$\frac{\partial T}{\partial X} = 0$,	$X = 0$,
	$T = 0$,	cold part	$\frac{\partial T}{\partial X} = 0$,	$X = 1$,
		$\frac{\partial T}{\partial X} = 0$,	$X = 0$ and 1,	$0 \leqslant Y \leqslant 1$.

The non-dimensional parameters that appear in the equations are, $Gr = \frac{g\beta(\theta_h - \theta_c)L^3}{\nu^2}$ Grashof number, $Ha^2 = \frac{B_0^2 L^2 \sigma_e}{\mu}$ Hartmann number, 2Ω period and $Pr = \frac{\nu}{\alpha}$ Prandtl number. The local Nusselt number is defined by $Nu = \frac{\partial T}{\partial X}|_{Y=0}$ resulting in the average Nusselt number as $\overline{Nu} = \int_h Nu dY$, where h $= \frac{L}{2}$ is height of heating location.

3. Method of solution

The governing Eqs. (5)–(8) are discretized by control volume method and solved by SIMPLE algorithm Patankar [15]. The discretized form of the Eq. (6) can be written as

$$\frac{\phi_P - \phi_P^0}{\Delta\tau}\Delta V + [(U\phi)_e - (U\phi)_w]\Delta Y + [(V\phi)_n - (V\phi)_s]\Delta X = \Gamma^\phi\left[\left(\frac{\partial\phi}{\partial X}\right)_e - \left(\frac{\partial\phi}{\partial X}\right)_w\right]\Delta Y + \Gamma^\phi\left[\left(\frac{\partial\phi}{\partial Y}\right)_n - \left(\frac{\partial\phi}{\partial Y}\right)_s\right]\Delta X + S^\phi(X, Y), \tag{9}$$

where $S^\phi(X,Y)$ is source term.

The third order accurate deferred QUICK scheme of Hayase et al. [16] is employed to minimize the numerical diffusion for the convective terms to the discretized Eq. (9) to obtain the form

$$a_P\phi_P^n = a_E\phi_E^n + a_W\phi_W^n + a_N\phi_N^n + a_S\phi_S^n + b_E\phi_E^{n-1} + b_W\phi_W^{n-1} + b_N\phi_N^{n-1} + b_S\phi_S^{n-1} + b_{EE}\phi_{EE}^{n-1} + b_{WW}\phi_{WW}^{n-1} + b_{NN}\phi_{NN}^{n-1} + b_{SS}\phi_{SS}^{n-1} + b_p\phi_p^{n-1} + S^\phi(X, Y).$$

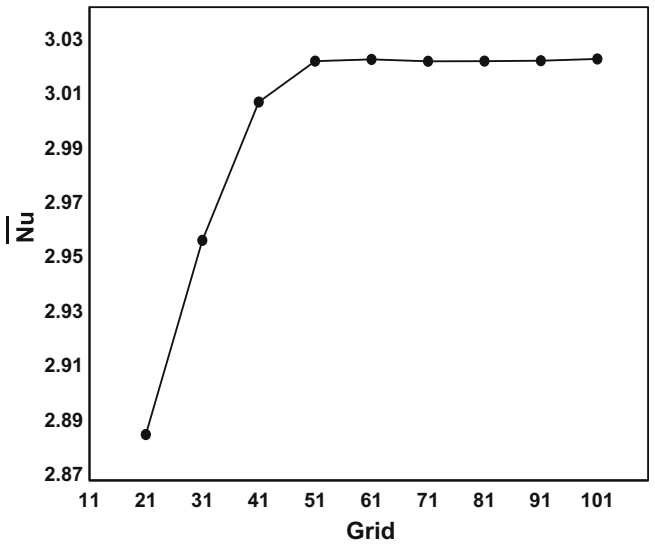

Fig. 2. Average Nusselt number for different grid sizes, middle–middle active walls, $A = 0$, $\Omega = 0$ and $Gr = 10^5$.

where

$$a_E = D_e + [|0, -F_e|], \quad a_W = D_w + [|0, F_w|]$$
$$a_N = D_n + [|0, -F_n|], \quad a_S = D_s + [|0, F_s|]$$
$$a_P = a_E + a_W + a_N + a_S + a_P^0$$
$$b_E = \frac{1}{8}\{-3[|0, F_e|] - 2[|0, -F_e|] + [|0, -F_w|]\}$$
$$b_W = \frac{1}{8}\{-3[|0, -F_w|] - 2[|0, F_w|] + [|0, F_e|]\}$$
$$b_N = \frac{1}{8}\{-3[|0, F_n|] - 2[|0, -F_n|] + [|0, -F_s|]\}$$
$$b_S = \frac{1}{8}\{-3[|0, -F_s|] - 2[|0, F_s|] + [|0, F_n|]\}$$
$$b_{EE} = \frac{-1}{8}[|0, -F_e|], \quad b_{WW} = \frac{-1}{8}[|0, F_w|]$$
$$b_{NN} = \frac{-1}{8}[|0, -F_n|], \quad b_{SS} = \frac{-1}{8}[|0, F_s|]$$
$$b_P = b_E + b_W + b_N + b_S + b_{EE} + b_{WW} + b_{NN} + b_{SS} + a_P^0.$$

The resulting set of discretized equations for each variable are solved by a line-by-line procedure, combining the tri-diagonal matrix algorithm (TDMA). Under relaxation technique is employed for the pressure correction. The mass balance for global convergence is taken as 10^{-7}.

Uniform staggered grid system is employed in the present study. The numerical solutions presented in this paper are acquired using 51×51 grid system. Further increase in the number of grids, produced essentially the same results as seen in Fig. 2. Accuracy of the numerical procedure is first validated by comparing the predicted results with the bench mark solutions of Davis [17] and the experimental investigation of Bairi [18]. The results are given

Table 1
Comparison of average Nusselt numbers for different Rayleigh number, $Pr = 0.71$ and $Ha = A = \Omega = 0$.

Ra	$\overline{Nu}$		
	Davis [17]	Bairi [18]	Present
10^3	1.116	1.112	1.119
10^4	2.234	2.168	2.259
10^5	4.487	4.228	4.518
10^6	8.811	8.243	8.851

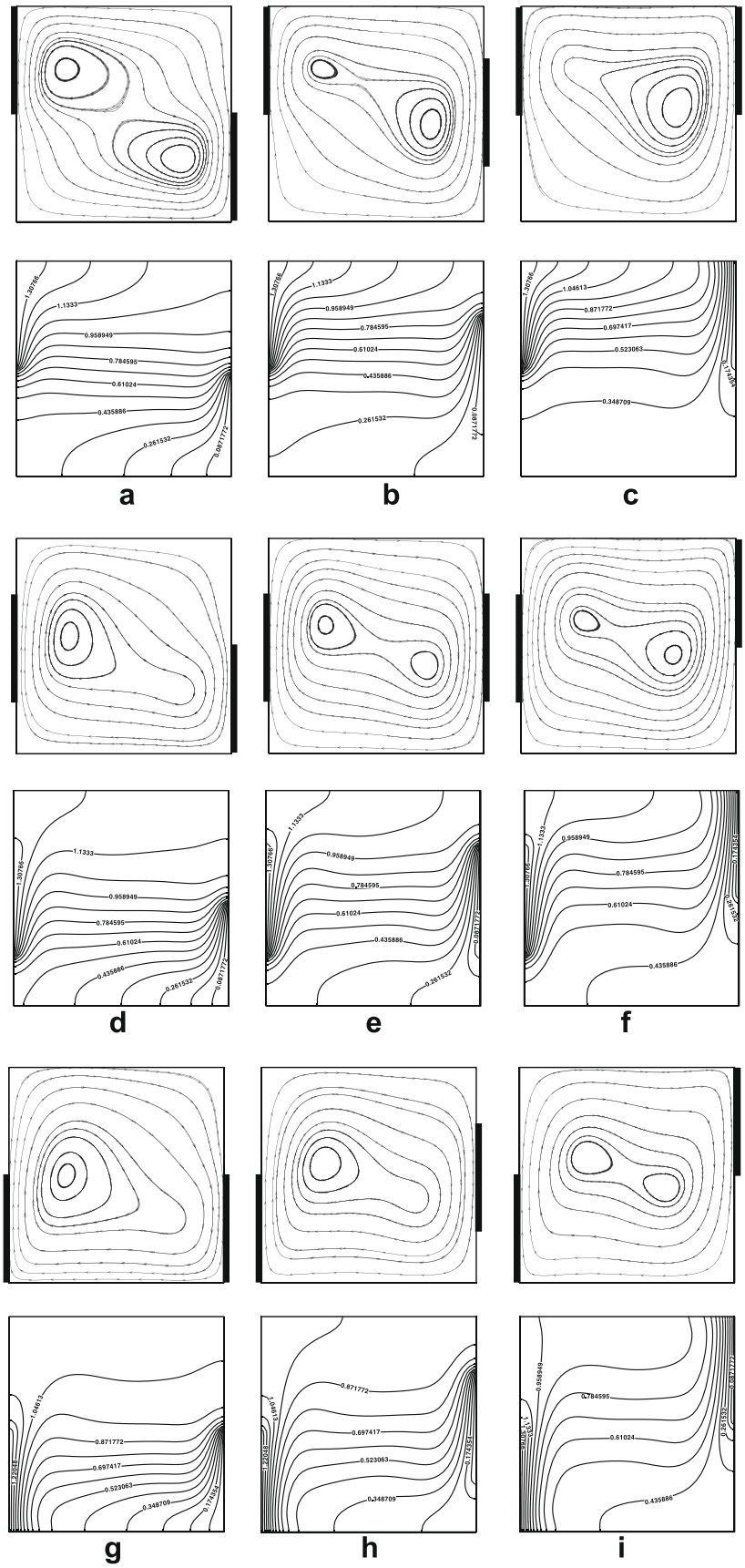

Fig. 3. (a–i) Streamlines and isotherms for nine combinations of active walls for $Gr = 10^5$, $Pr = 0.71$, $Ha = 10$, $A = 0.4$, $\Omega = 3$.

in Table 1 and we can see that the present values of average Nusselt number are in good agreement with those obtained by various authors. We are, therefore, confident that the results reported in our paper are accurate.

4. Results and discussion

The magnetoconvection of an electrically conducting fluid in a square cavity is studied numerically for nine different combinations of thermally active locations. The computations are carried out for various values of the Grashof number from 10^4 to 10^6, Hartmann number from 0 to 100, Prandtl number from 0.054 to 2.05, amplitude from 0.2 to 0.6 and period from 1 to 5, of the time periodic hot zone.

Fig. 3a–i depicts the streamlines and isotherms for $Gr = 10^5$, $A = 0.4$, $\Omega = 3$, $Ha = 10$ and $Pr = 0.71$ for different combinations of the active locations. As the left top active location is at a higher temperature the adjoining fluid particles gets heated up, undergo the drop in their densities and raise above their mean level and travel to the right active cold location and produces a clockwise rotating cell within which two smaller clockwise rotating cells due to the same reasoning appear with a small stagnant region between them avoiding shear instability. The flow and the temperature field are symmetric with respect to the plane $Y = 0.5$ (see Fig. 3a).

As the cold location is moved to the middle and top positions the hot cell is squeezed and disappears to produce elongated single cell pattern. The corresponding isotherms indicate convective mode of heat transfer at the active regions in Fig. 3b and c . In the middle heating position the initial single cell formation splits into dual cells within the larger flattened cell in Fig. 3d–f. The corresponding isotherms in Fig. 3d–f shows that convective mode prevails everywhere inside the cavity with a thin thermal boundary layer at the middle–top active locations.

In the bottom heating location in Fig. 3(g–i) and the reversal of the top hot–bottom cold case prevails but for the thick thermal boundary layer formation. The convective regime is well established in this case. Fig. 4(a–d) and exhibit the streamlines and isotherms for the top hot–bottom cold active locations with $A = 0.4$, $Gr = 10^5$, $Ha = 10$, $Pr = 0.71$ and Ω varying as 1, 2, 4 and 5. As the period increases the unicellular pattern turns out to be multicellular and the dual cells separate the flow at the core as seen in Fig. 4d at $\Omega = 5$. The corresponding isotherms exhibit clearly the convective mode of heat transfer within the cavity except at the core.

Fig. 5(a–l) indicate the streamlines and the isotherms for $\Omega = 3$, $Gr = 10^5$, $Pr = 0.71$, $A = 0.2$, 0.4 and 0.6, for the bottom hot–top cold active locations. The flow starts with a major convective cell with tiny inner cells. As the Hartmann number increases they develop to form a conductive regime is established with the two inner cells enlarged and fully developed at the center of the cavity as in Fig. 5(a–l). The isotherms Fig. 5(a–l) indicate that the warm fluid confined to the boundary layer is entrained to the whole cavity yet convection is retarded by the increase in the applied magnetic field. This is clear from the almost parallel, straightened horizontal isotherms, reflecting nearly conductive mode of heat transfer within the cavity which is also quantitatively observed from Table 2.

Fig. 6 illustrates the transient results of streamlines and isotherms for $Gr = 10^5$, $Ha = 10$, $Pr = 0.71$, $\Omega = 3$, $A = 0.4$ and for bottom hot–top cold active locations. In the initial stage a small amount of fluid near the hot region is activated. For $\tau = 0.002$ a small clockwise rotating hot cell appears near the bottom heating locations and the isotherms are almost parallel lines. They indicate conduction mode of heat transfer. At times 0.008 and 0.016 the clockwise rotating cell grows in size, moves slightly away from the boundary and expands, while the isotherms become parabolic and spreads to more than half of the cavity. When $\tau = 0.032$ and 0.064 the convective cell has moved to the center, elongated to elliptic shape and occupies the entire cavity. The corresponding isotherms have reached the right side top cooling location which are tilted at the core region. As τ increases further to 0.128 and 1.024 the inner cell splits into two and the streamlines are suppressed horizontally, the isotherms at the core become horizontal and the thermal boundary layer is well established showing the development of the convective mode of heat transfer.

Fig. 7 indicates the time history of the mid-height velocity profiles for the transient state for $Gr = 10^5$, $Ha = 10$, $Pr = 0.71$, $\Omega = 3$, $A = 0.4$ and for bottom hot–top cold active locations. Initially the

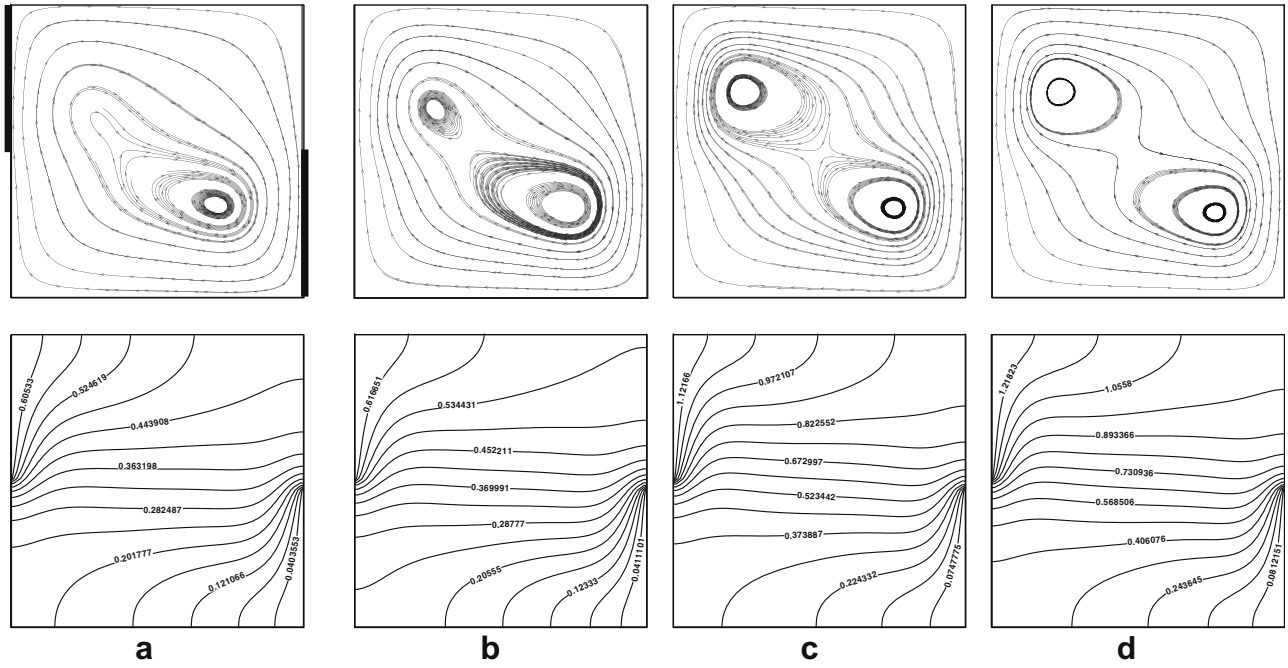

Fig. 4. (a–d) Streamlines and isotherms for top–bottom active walls, for $Gr = 10^5$, $Pr = 0.71$, $Ha = 10$, $A = 0.4$ and $\Omega = 1$, 2, 4 and 5.

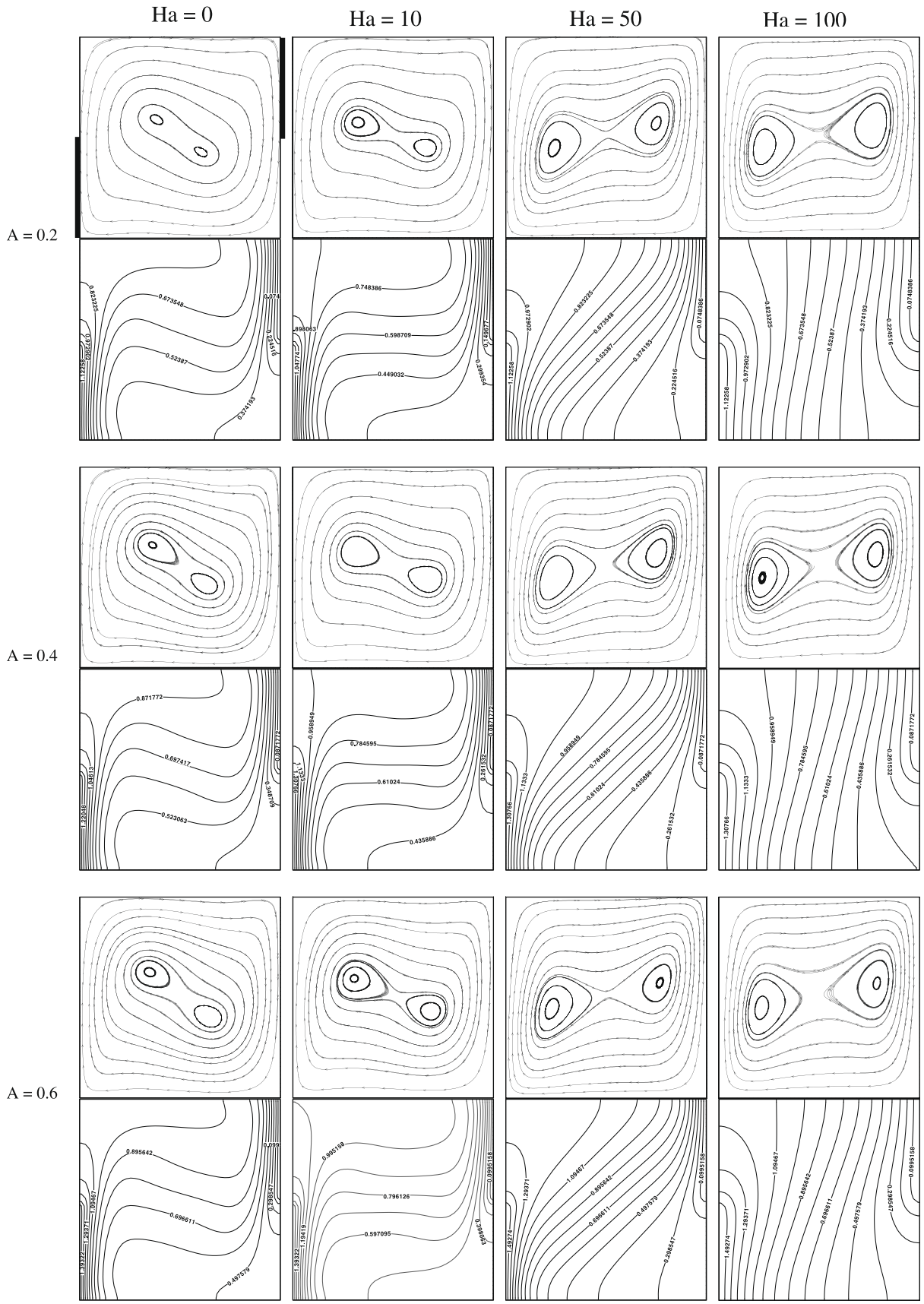

Fig. 5. (a–l) Streamlines and isotherms for bottom–top active walls, different *Ha*, different *A*, $\Omega = 3$, $Pr = 0.71$ and $Gr = 10^5$.

Table 2
Effect of Grashof number and Hartmann number on average Nusselt number, horizontal and vertical velocities for bottom–top active location, $A = 0.4$, $\Omega = 3$, $Pr = 0.71$ and $Ha = 10$.

Gr	Ha	U_{max}	V_{max}	Avg. Nu
10^4	0	18.53	22.48	4.001632
	10	12.90	16.67	3.511169
	50	1.59	2.56	1.908844
	100	0.36	0.92	1.861611
10^5	0	49.02	89.90	7.670641
	10	45.28	78.01	7.568953
	50	17.28	33.10	4.736051
	100	5.31	11.21	2.329440
10^6	0	185.25	319.14	15.376016
	10	140.78	316..40	15.275935
	50	62.73	222.49	15.110399
	100	49.25	146.03	11.978464

velocity increases only near the hot location, when time evolves the temperature of the fluid particles near the cold location also increased and the velocity curves coincide once the steady state is reached. The variation in the average Nusselt number for the increase in Prandtl number are shown in Fig. 8 for different heating locations, for $Ha = 10$, $Gr = 10^5$, $\Omega = 3$ and $A = 0.4$. The rate of increase is high in the range $Pr = 0.054$–0.71. It is also observed that in the middle–middle active locations the heat transfer rate is more than in the other cases.

Fig. 9 presents the variation of the average Nusselt number with Hartmann numbers for different values of Ω, $Gr = 10^5$, $A = 0.4$, $Pr = 0.71$ and for the bottom hot–top cold active locations. The average Nusselt number reduces significantly as the Hartmann number increases. As Ω increases the average Nusselt number oscillates. The effect is found to be maximum for $\Omega = 3$ and less for all other cases.

Fig. 10 shows the variation of the average Nusselt number with Hartmann numbers for various values of amplitude A and $Gr = 10^5$, $\Omega = 3$, $Pr = 0.71$ and for the bottom hot–top cold active locations. As A increases the average Nusselt number also increases for lower values of Hartmann number. But as Hartmann number increases, the rate of heat transfer is sharply reduced. Fig. 11 indicates the variations of the average Nusselt number with Grashof number for several values of Ha. The effect of magnetic field on the average

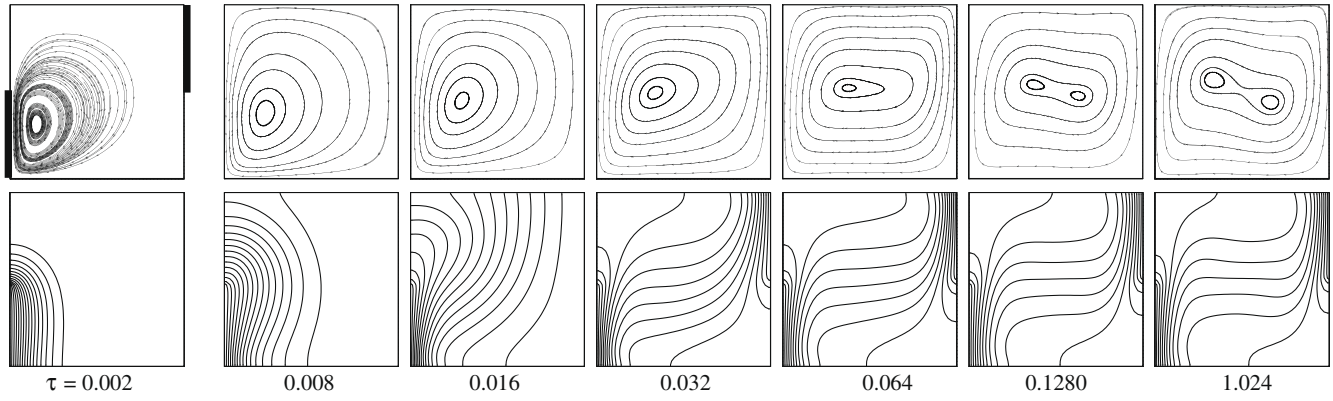

Fig. 6. Time history of streamlines and isotherms for bottom–top active walls, $Pr = 0.71$, $Ha = 10$, $A = 0.4$, $\Omega = 3$ and $Gr = 10^5$.

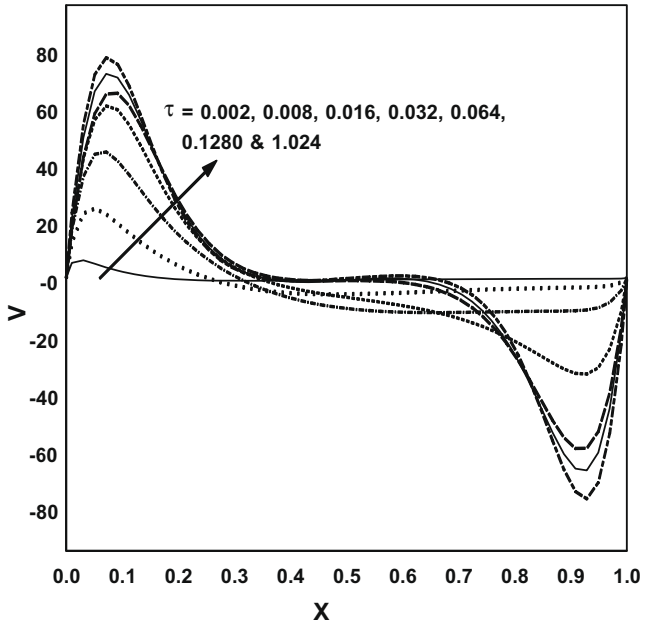

Fig. 7. Time history of mid-height velocity profile for bottom–top active walls, $Pr = 0.71$, $A = 0.4$, $\Omega = 3$, $Ha = 10$ and $Gr = 10^5$.

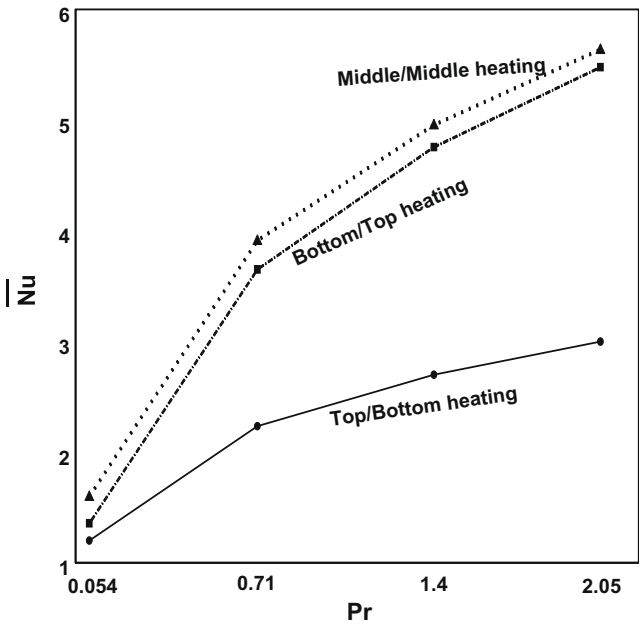

Fig. 8. Average Nu vs Pr for different active walls, $Gr = 10^5$, $A = 0.4$, $\Omega = 3$ and $Ha = 10$.

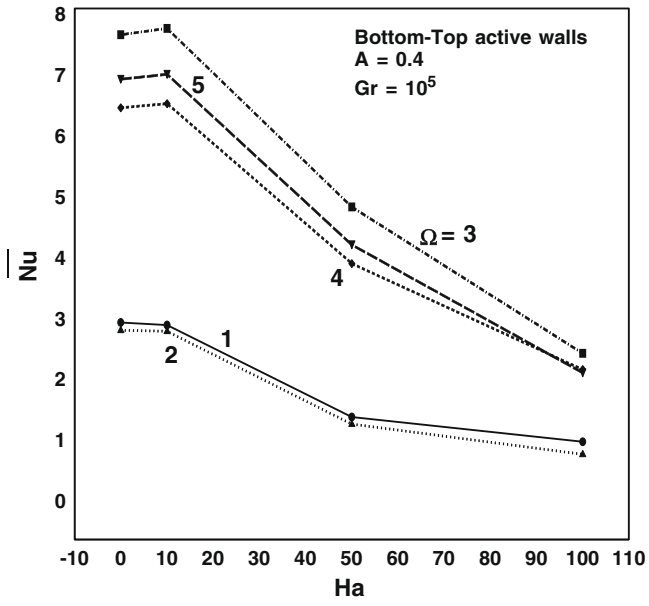

Fig. 9. Average *Nu* vs *Ha* for different period Ω and *Pr* = 0.71.

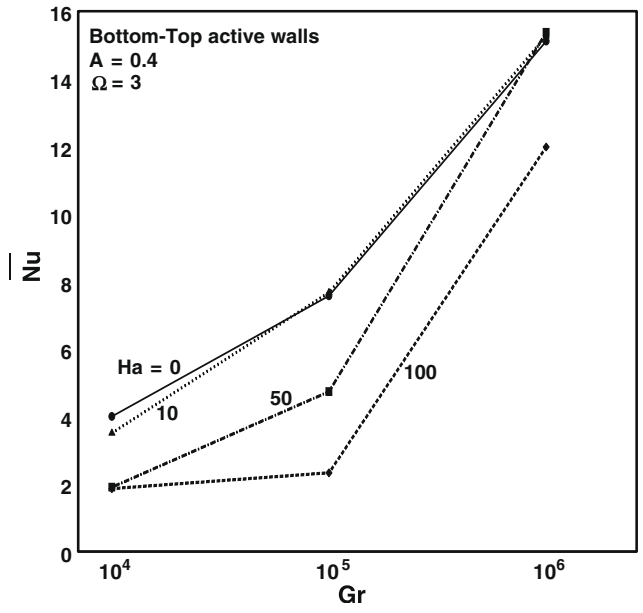

Fig. 11. Average *Nu* vs *Gr* for different *Ha* and *Pr* = 0.71.

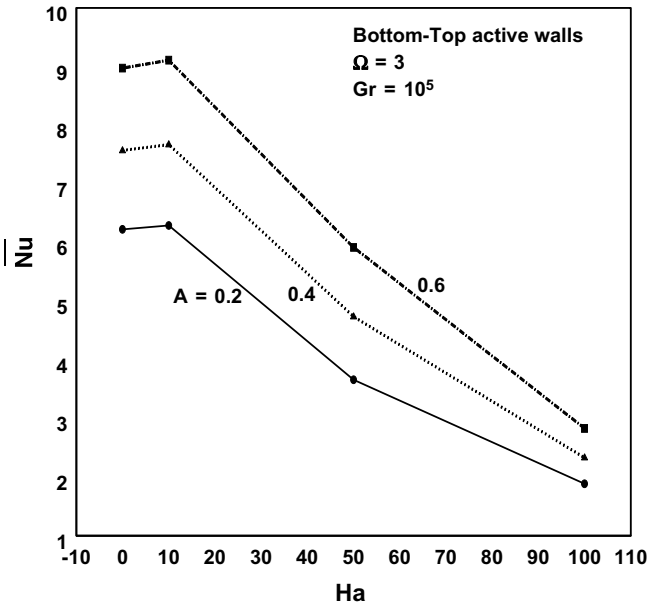

Fig. 10. Average *Nu* vs *Ha* for different amplitudes *A* and *Pr* = 0.71.

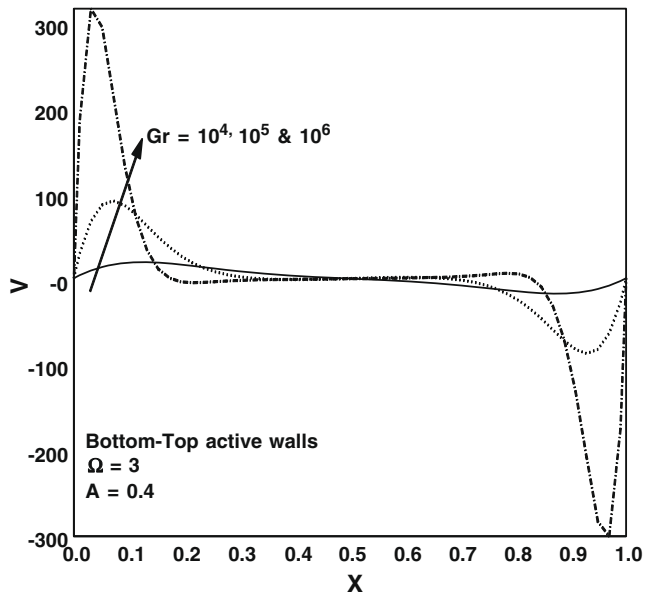

Fig. 12. Mid-height vertical velocity profiles for different *Gr* and *Pr* = 0.71.

Nusselt number is more in the lower Grashof number region. At higher Grashof number values, as convection is dominant the reduction in heat transfer due to magnetic field is insignificant except for *Ha* = 100.

Fig. 12 shows the vertical velocity profiles at mid-height for various values of Grashof number, Ω = 3, *A* = 0.4, *Ha* = 10, *Pr* = 0.71 for bottom hot–top cold active positions. The flow is invigorated for $Gr = 10^6$ but suppressed for 10^4.

Fig. 13 exhibits the vertical velocity profiles at mid-height for periods from 1 to 5. As period increases the velocity profiles oscillate and attains extreme values for Ω = 3 for the bottom hot–top cold active positions. The increase in Ha reduces the peaks near the active walls as seen in Fig. 14 for $Gr = 10^5$, Ω = 3, *A* = 0.4 for bottom hot–top cold active locations, showing that the convective mode of heat transfer is transformed to conductive mode.

Fig. 15 shows the steady state average Nusselt number variations for $Gr = 10^5$, Ω = 3, *A* = 0.4, *Ha* = 10, *Pr* = 0.71 and for bottom hot–top cold active locations. There is a sudden drop in the value of the average Nusselt number in the initial stage. When the steady state is reached the average Nusselt number oscillates steadily and asymptotically.

5. Conclusion

In this study numerical results of magnetoconvection in a square cavity subjected to sinusoidal temperature boundary conditions on the heating location of one of the side walls are presented. Liquid metals (*Pr* = 0.054) is used as a coolant in nuclear reactors for thermodynamics systems. It is observed that the heat transfer rate is enhanced in the middle–middle thermally active locations.

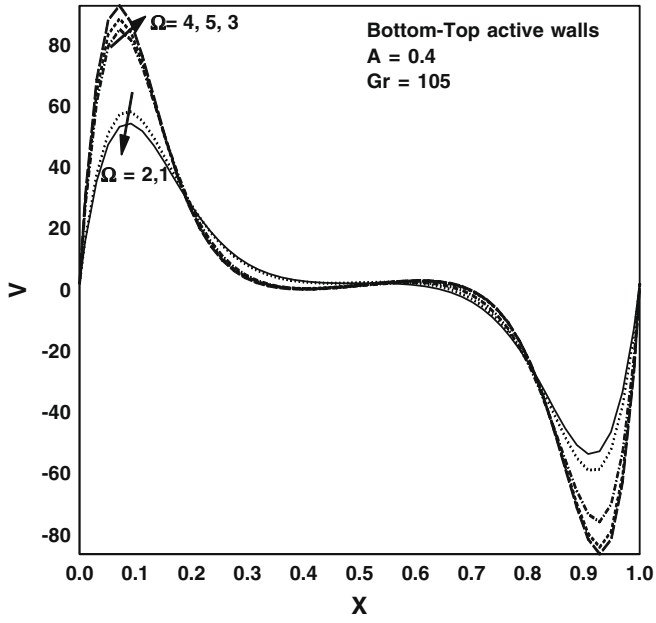

Fig. 13. Mid-height vertical velocity profiles for different periods Ω, $Ha = 10$ and $Pr = 0.71$.

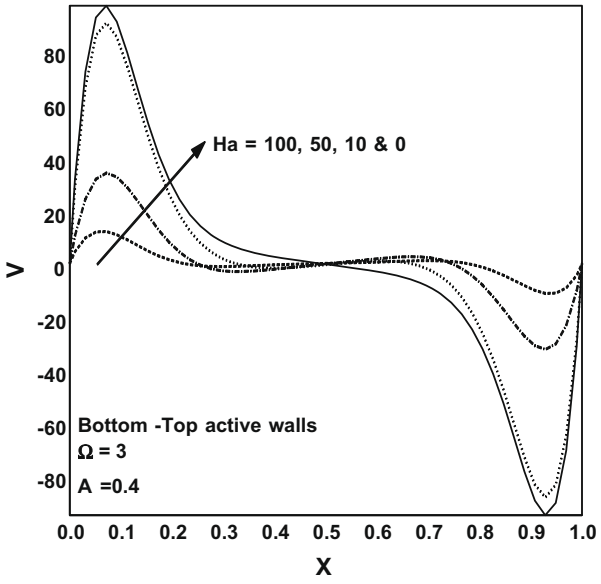

Fig. 14. Mid-height vertical velocity profiles for different Ha and $Pr = 0.71$.

The average Nusselt number increases with increase in Prandtl number and Grashof number and decreases with Hartmann number. The rate of heat transfer and vertical velocity oscillates for increasing amplitudes but it is maximum for $\Omega = 3$ and increases for increase in period. As A increases the average Nusselt number also increases for lower values of Hartmann number. But as Hartmann number increases, the rate of heat transfer is sharply reduced. The flow is invigorated for $Gr = 10^6$ but suppressed for 10^4. In the steady state the rate of heat transfer resonates to the periodic temperature at the hot region. For sufficiently large magnetic field $Ha = 100$ the convective mode of heat transfer is converted into conductive mode.

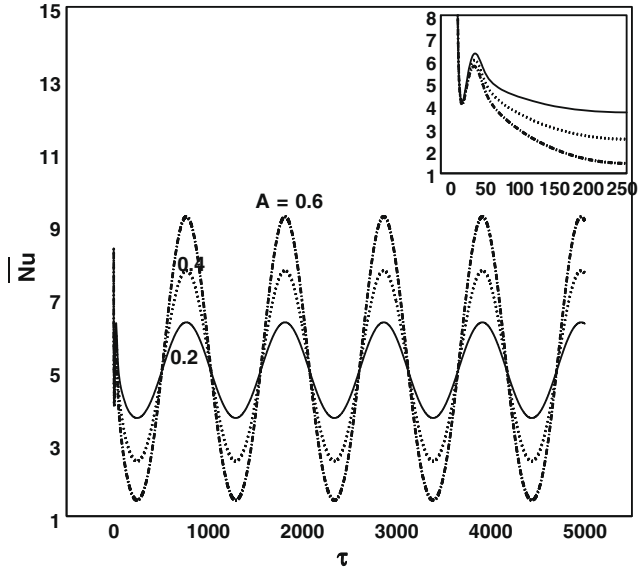

Fig. 15. Average Nusselt number vs time τ for bottom–top active location, $Pr = 0.71$, $Ha = 10$, $\Omega = 3$ and $Gr = 10^5$.

References

[1] J.L. Lage, A. Bejan, The resonance of natural convection in an enclosure heated periodically from the side, Int. J. Heat Mass Transfer 36 (1993) 2027–2038.

[2] N. Rudraiah, R.M. Barron, M. Venkatachalappa, C.K. Subbaraya, Effect of a magnetic field on free convection in a rectangular enclosure, Int. J. Eng. Sci. 33 (1995) 1075–1084.

[3] H.S. Kwak, K. Kuwahara, J.M. Hyun, Predictions of the resonance frequency of natural convection in an enclosure with time-periodic heating imposed on one sidewall, Int. J. Heat Mass Transfer 41 (1998) 3157–3160.

[4] P. Kandaswamy, K. Kumar, Buoyancy-driven nonlinear convection in a square cavity in the presence of a magnetic field, Acta Mech. 136 (1999) 29–39.

[5] H.P. Oosthuizen, T.J. Paul, Unsteady natural convection flow in an enclosure with two heated side wall sections, in: Proceedings of the National Heat Transfer Conference, ASME, NHTC 99-291, 1999, pp. 1–8.

[6] G.B.L. Kim, J.M. Hyun, H.S. Kwak, Enclosed buoyant convection with internal heat generation under oscillating sidewall temperature, J. Heat Transfer 124 (2002) 577–580.

[7] N.H. Saeid, Natural convection in porous cavity with sinusoidal bottom wall temperature variation, Int. Commun. Heat Mass Transfer 32 (2005) 454–463.

[8] D.W. Crunkleton, R. Narayanan, T.J. Anderson, Numerical simulations of periodic flow oscillations in low Prandtl number fluids, Int. J. Heat Mass Transfer 49 (2006) 427–438.

[9] N. Nithyadevi, P. Kandaswamy, S. Sivasankaran, Natural convection in a square cavity with partially active vertical walls: time periodic boundary condition, Math. Probl. Eng. 2006 (2006) 1–16.

[10] E. Bilgen, R. Ben Yedder, Natural convection in enclosure with heating and cooling by sinusoidal temperature profiles on one side, Int. J. Heat Mass Transfer 50 (2007) 139–150.

[11] N.B. Cheikh, B.B. Beya, T. Lili, Aspect ratio effect on natural convection flow in a cavity submitted to a periodical temperature boundary, J. Heat Transfer 129 (2007) 1060–1068.

[12] N. Nithyadevi, P. Kandaswamy, J. Lee, Natural convection in a rectangular cavity with partially active side walls, Int. J. Heat Mass Transfer 50 (2007) 4688–4697.

[13] E. Natarajan, T. Basak, S. Roy, Natural convection flows in a trapezoidal enclosure with uniform and non-uniform heating of bottom wall, Int. J. Heat Mass Transfer 51 (2008) 747–756.

[14] P. Kandaswamy, S. Malliga Sundari, N. Nithyadevi, Magnetoconvection in an enclosure with partially active vertical walls, Int. J. Heat Mass Transfer 51 (2008) 1946–1954.

[15] S.V. Patankar, Numerical Heat Transfer and Fluid Flow Hemisphere, McGraw-Hill, Washington, DC, 1980.

[16] T. Hayes, J.A.C. Humphrey, R. Greif, A consistently formulated QUICK scheme for fast and stable convergence using finite volume iterative calculation procedures, J. Comput. Phys. 98 (1992) 108–118.

[17] G. Davis, Natural convection of air in a square cavity: a bench mark numerical solution, Int. J. Numer. Meth. Fluids 3 (1983) 249–264.

[18] A. Bairi, Nusselt–Rayleigh correlations for design of industrial elements: experimental and numerical investigation of natural convection in tilted square air filled enclosures, Energy Convers. Manage. 49 (2008) 771–782.